Electrochemical and Spectroscopic Study of Benzotriazole Films Formed on Copper, Copper-zinc Alloys and Zinc in Chloride Solution

I. Milošev[a,b,*] and T. Kosec[a]

[a] Jožef Stefan Institute, Department of Physical and Organic Chemistry, Jamova 39, 1000 Ljubljana, Slovenia

[b] Orthopaedic Hospital Valdoltra, Jadranska c. 31, 6280 Ankaran, Slovenia

Original scientific paper
Received: July 2, 2008
Accepted: December 11, 2008

The formation of protective layers on copper, zinc and copper-zinc (Cu-10Zn and Cu-40Zn) alloys at open circuit potential in aerated, near neutral 0.5 M NaCl solution containing benzotriazole (BTA) was studied using potentiodynamic measurements, electrochemical impedance spectroscopy (EIS) and X-ray photoelectron spectroscopy (XPS). The addition of benzotriazole affects the dissolution of the materials investigated. Benzotriazole, generally known as an inhibitor of copper corrosion, is also shown to be an efficient inhibitor for copper-zinc alloys and zinc metal. The effectiveness of inhibition depending on the type of materials was compared. X-ray photoelectron spectroscopic results showed that the surface layer formed on alloys in BTA-inhibited solution comprised both oxide and polymer components. The formation of Cu_2O/Cu(I)-BTA on copper, mixed oxides/Zn(II)-BTA and Cu(I)-BTA on copper-zinc alloys and ZnO/Zn(II)-BTA polymer surface film on zinc provides an effective barrier against corrosion on materials investigated in chloride solution.

Key words:
Copper, brass, zinc, benzotriazole, inhibition, EIS, XPS

Introduction

Understanding the inhibition mechanism of a corrosion process on a micro scale enables to find versatile ways of material and metal protection in order to prevent or postpone the attack of corrosion. Inhibitors are chemical substances that react with the surface of the metal or they may effect the corrosion media to which the metal specimen is subjected. Different environments require versatile inhibition actions. Benzotriazole (BTAH) is known as a yellow brass inhibitor, even though the majority of investigations were conducted on copper.[1–8] Despite many investigations, it is still a matter of debate whether the inhibitive film exists as Cu(I)-BTA complex, adsorbed BTAH film or BTA polymer structure.[9] Due to less extensive investigations on brass,[10–14] the aim of this work was to study the inhibition efficiency of benzotriazole on copper-zinc alloys and zinc metal.

Experimental

Materials and solutions

Copper (99.95 %) and zinc (99.5 %) sheets were purchased from Goodfellow Cambridge Ltd., UK). Copper-zinc alloys, Cu-10Zn and Cu-40Zn, denoted by wt. %, were supplied by Wieland-Werke AG, Ulm, Germany. Samples were sectioned from 2-mm sheets in the form of discs of 14 mm diameter and served as working electrodes. Prior to measurement, the specimens were abraded with 1000, 2400 and 4000-grid emery paper, ultrasonically cleaned in distilled water for 2 minutes, and dried well.

Measurements were conducted in aerated 0.5 M NaCl solution prepared from analytical grade chemical and distilled water. The prepared solution had an initial pH value of 6.4. Benzotriazole (BTAH) of purity >99 % was obtained as a white granulated powder from Merck, Schuchardt, Germany. It was added to the NaCl solution to give 0.05, 1, and 10 mM BTAH.

Electrochemical measurements

An Autolab three-electrode corrosion cell was used, with the working electrode embedded in a Teflon holder, exposing an area of 0.785 cm^2. A saturated calomel electrode (SCE) served as a reference electrode and two stainless steel rods as counter electrodes. Potentials are reported with respect to the SCE scale. An Autolab PGSTAT12 potentiostat/galvanostat, expanded with an FRA2 module, was used for electrochemical measurements.

Following a 1 h stabilization at open circuit potential (OCP), potentiodynamic polarization curves

*Corresponding author. Tel.: +386-1-4773-452; fax: +386-1-4773-822; E-mail: ingrid.milosev@ijs.si

were measured starting from –250 mV versus OCP up to 1.1 V using scan rate of 1 mV s^{-1}. All the measurements were performed at room temperature in well-aerated solution.

Electrochemical impedance spectroscopy (EIS) was performed in the frequency range from 65 kHz to 5 mHz at 10 cycles per decade with an *ac* amplitude of ± 10 mV. The absolute impedance and phase angle were measured at each frequency. The impedance measurements were carried out at the open circuit potential after 2 h immersion in the electrolyte. Measurements were performed in 0.5 M NaCl in the presence and absence of 0.05 mM and 10 mM BTAH. The impedance data were interpreted on the basis of equivalent electrical circuits, using the Zview (Scribner) program for fitting the experimental data.

X-ray photoelectron spectroscopy (XPS)

XPS spectra were recorded on surface films formed on Cu, Cu-10Zn, Cu-40Zn and Zn during 2 h immersion at the open circuit potential in 0.5 M NaCl containing 10 mM BTAH. After rinsing, the samples were dried and stored under an inert atmospheric until XPS analysis was performed.

XPS was performed with a TFA Physical Electronics Inc. spectrometer using monochromatized Al Kα radiation (1486.6 eV) and a hemispherical analyzer. A take-off angle, defined as the angle of emission to the surface, of 45° was used. The energy resolution was 0.5 eV. Survey scan spectra were recorded at a pass energy of 187.85 eV, whereas individual high resolution spectra were taken at a pass energy of 23.5 eV with an energy step of 0.1 eV. After taking the surface spectra, depth profiling of the oxidized layers was performed. An Ar^+ ion beam with an energy level of 1 keV and a raster of 3 mm × 3 mm was used for sputtering. This resulted in a sputtering rate of 1 nm min^{-1} relative to the Ta_2O_5 standard.[15] Generally, the depth at which the intensity of oxygen decreases to a half, or the depth at which the intensity of nitrogen diminishes is taken as a measure of film thickness.

Cu and Zn XPS spectra were deconvoluted as described in detail.[16] The Cu $2p_{3/2}$ peak cannot be used to differentiate between Cu metal and cuprous oxide due to the small chemical shift between the two. These species can be differentiated on the basis of Auger [$Cu(L_3M_{4,5}M_{4,5})$] spectra. The metal shows a main Auger peak at E_b of 568.2 eV, while in Cu_2O this peak is located at 570.6 eV. As with copper, Auger [$Zn(L_3M_{4,5}M_{4,5})$] spectra enabled Zn and ZnO to be differentiated. The Auger line for Zn is identified at an E_b value of 494.4 eV, and that for ZnO at 499.1 eV. In contrast, the chemical shift between Zn and ZnO XPS $2p_{3/2}$ peaks do not enable differentiation between these two oxidation states.[16] The position of the N 1s peak in an organic matrix is expected at binding energies between 397.9 and 401 eV.[17]

Results and discussion

Potentiodynamic polarization curves

In the course of prolonged immersion at OCP in aerated chloride solution under slightly acidic solution, copper can oxidize:[18]

$$2\ Cu + \tfrac{1}{2}O_2 + 2\ H^+ \rightarrow 2\ Cu^+ + H_2O \qquad (1)$$

Cu^+ can be present as $Cu(OH)_{ads}$ or Cu_2O.[8,19] Chloride ions can adsorb on the $Cu(OH)_{ads}$ to form an adsorbed complex:

$$Cu(OH)_{ads} + Cl^- \rightarrow CuCl_{ads} + OH^- \qquad (2)$$

Following the immersion at OCP, the sample is subjected to potentiodynamic polarization. The potentiodynamic curves for Cu, Zn, Cu-10Zn and Cu-40Zn alloys in 0.5 M NaCl in the presence and absence of benzotriazole are presented in Fig. 1. Since the polarization started from cathodic potentials, a part of oxide formed during immersion is reduced. The unreduced part remains at the surface and may induce a departure from anodic Tafel slope of approximately 60 mV which is usually observed in chloride solution.[19] The corrosion potential, E_{corr}, of copper, –0.235 V, is somewhat more negative than those of the two alloys, –0.220 V and –0.210 V for the Cu-10Zn and Cu-40Zn alloy, respectively. The corrosion potential for zinc is the most negative, –1.08 V.

The Tafel region of copper and copper alloys is limited by peak current at approximately 0.1 V which is associated with the CuCl formation[7] for copper and alloys:

$$CuCl + Cl^- \rightarrow CuCl_2^- \qquad (3)$$

The equilibrium between Cu and CuCl is given by the reaction:

$$Cu + Cl^- \rightarrow CuCl_{ads} + e^- \qquad (4)$$

The parallel dissolution of zinc in chloride solution follows the reaction:

$$Zn + 4Cl^- \rightarrow ZnCl_4^{2-} + 2\ e^- \qquad (5)$$

However, a certain amount of zinc atoms can be involved in the chemical reaction:[20]

$$2CuCl_2^- + Zn \rightarrow 2Cu + ZnCl_4^{2-} \qquad (6)$$

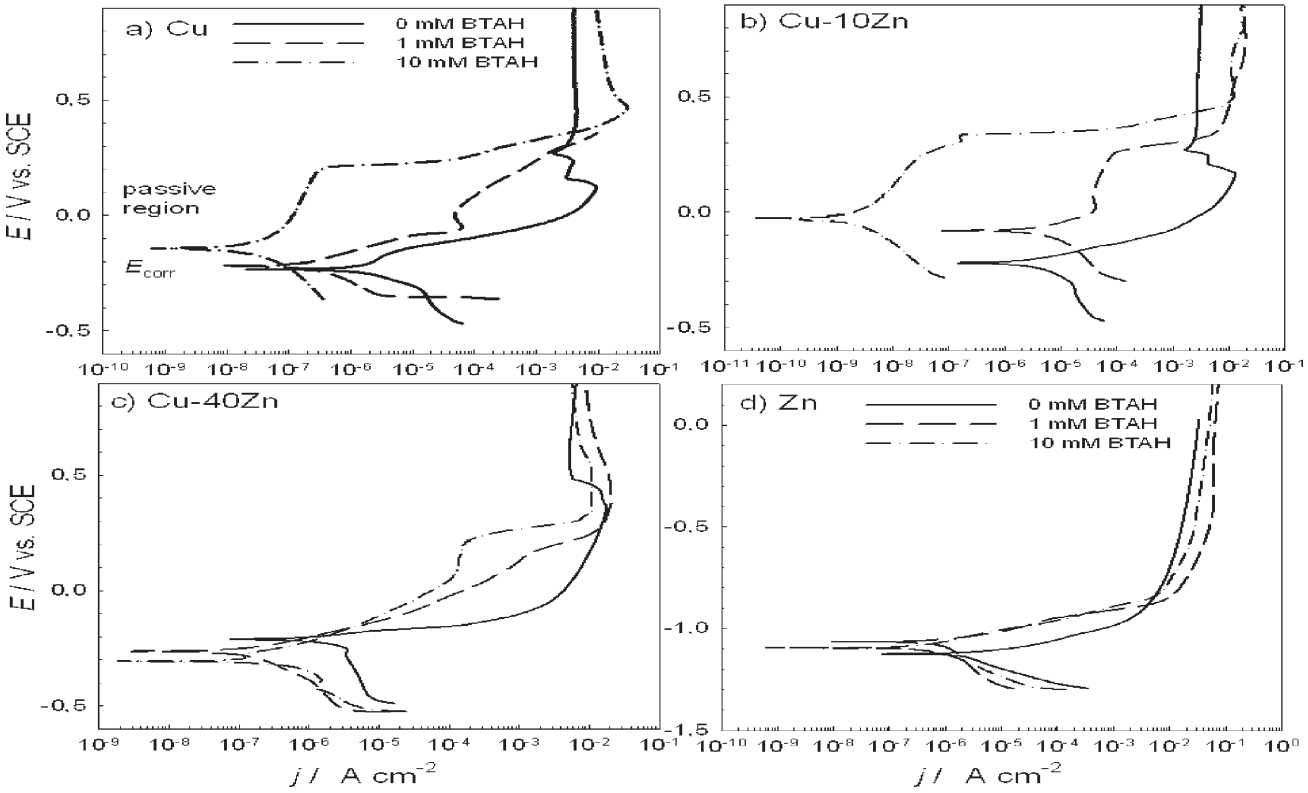

Fig. 1 – *Potentiodynamic curves for Cu, Cu-10Zn and Cu-40Zn alloys and Zn recorded in 0.5 M NaCl in the absence and presence of 1 mM and 10 mM BTAH. Electrodes were stabilized at OCP for 1 h. dE/dt = 1 mV s^{-1}.*

A current minimum at approximately 0.2 V for Cu and Cu-10Zn alloy is reached when the formation of CuCl is completed (Figs. 1a, b). Since the solubility product constant for CuCl is very low, K_{sp}[CuCl] = 1.72 · 10^{-7},[21] in chloride media it dissolves through complexation and forms stable complexes, reaction (3). Cuprous chloride complexes formed can either diffuse to bulk solution or oxidize to form cupric ions.[7]

Copper and both alloys show similar anodic behaviour, while zinc behaves differently (Fig. 1d). Following the corrosion potential of –1.08 V, the current density of zinc increases with potential in the Tafel region and then levels off at values higher than 0.01 A cm^{-2}.

Already the addition of 1 mM BTAH to NaCl solution induces a decrease in cathodic and anodic current densities of copper (Fig. 1a). The current density levels off at approx. –0.05 V and then increases again. For 10 mM BTAH, however, a true passive range is established up to 0.2 V with current densities up to 4 orders of magnitude lower than for BTAH-free solution. In the case of the Cu-10Zn alloy, BTAH-induced passivation is already observed at only 1 mM BTAH (Fig. 1b). For 10 mM BTAH, the passive range is extended up to 0.3 V, and much lower current densities are observed (Fig. 1b). For Cu-40Zn alloy (Fig. 1c), the decrease in current density is lower than for Cu and Cu-10Zn alloy. Zinc metal does not form any passive region in BTAH-containing solutions, but a decrease in current density in the entire potential range was observed (Fig. 1d). Generally, the corrosion potential moved to more positive values in the presence of the inhibitor (Fig. 1).

Electrochemical impedance spectroscopy

Impedance data in the form of Nyquist plots of Cu, Cu-10Zn and Cu-40Zn alloys and Zn after 2 h immersion at the OCP in 0.5 M NaCl are presented in Fig. 2. Impedance spectra for copper, its alloys with zinc and zinc consist of a high frequency intercept with the abscise axis and a middle frequency part. In the case of copper and Cu-10Zn alloy a low frequency arc, and loops in the case of zinc were observed. Equivalent circuits used to fit the data are shown in Fig. 1b and the parameters obtained are presented in Table 1. Equivalent circuits for fitting experimental data consisted of solution resistance R_e connected in series with two time constants $R_1[Q_1(R_2Q_2)]$. The symbols Q signify the possibility of a non-ideal capacitance (CPE, Constant Phase Element) with varying n. The impedance of the CPE is given by:[22]

$$Q = Z_{CPE}(\omega) = [C(j\omega)^n]^{-1}. \quad (7)$$

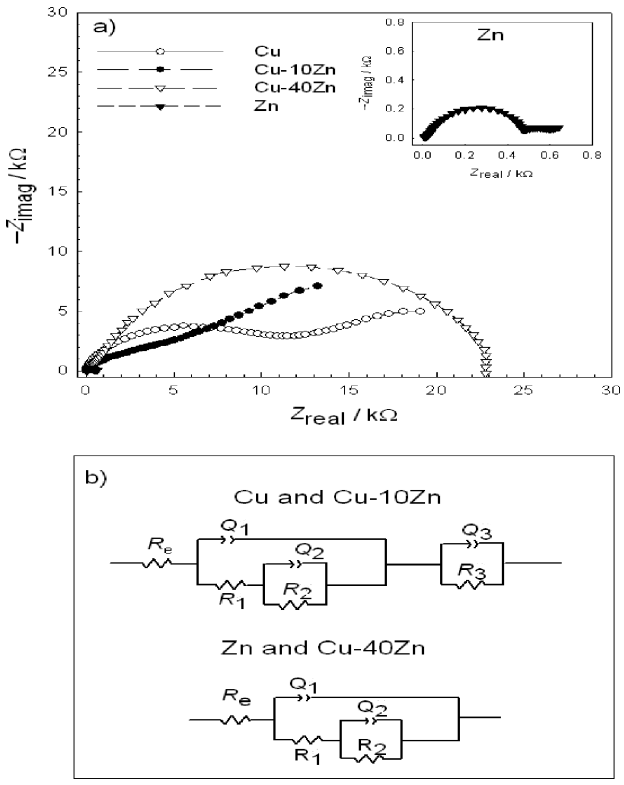

F i g . 2 – *(a) Experimental and fitted Nyquist plots for Cu, Cu-10Zn and Cu-40Zn alloys and Zn in 0.5 M NaCl after 2 h immersion. (b) Equivalent circuits used for spectra fitting.*

For $n = 1$, the Q element reduces to a capacitor with a capacitance C and, for $n = 0$, to a simple resistor. Copper and Cu-10Zn alloy behave similarly (Fig. 2a). Impedance response may be described by three processes. Parameter Q_1 represents the capacitive behaviour of the passive film formed, coupled with resistance due to ionic paths through oxide film R_1. In the second process, Q_2 represents the capacitive behaviour at the electrolyte/metal interface (i.e. the double layer) and R_2 represents the corresponding charge transfer resistance. Additional low frequency tail observed for Cu and Cu-10Zn alloy requires the introduction of the third time constant (R_3Q_3). The values of parameter n around 0.5 indicate the diffusion process of cuprous ions through the pores in oxide film.[23] The data for zinc were fitted in the range from 65 kHz to 1 Hz in order to omit the low frequency loop that should represent the dissolution of corrosion product into solution. This procedure did not affect the final result of polarization resistance.

The equivalent circuits and fitted curves for the experimental spectra for Cu, Cu-10Zn and Cu-40Zn alloys and zinc in the presence of two inhibitor concentrations, 0.5 and 10 mM, are presented in Fig. 3. The shape of EIS spectra is dependent on the inhibitor concentration. For example, in the case of Cu,

T a b l e 1 – *Fitting results of EIS spectra recorded for Cu, Cu-10Zn and Cu-40Zn alloys, and Zn after 2 h immersion in 0.5 M NaCl, and in 0.5 M NaCl containing 0.05 mM BTAH and 10 mM BTAH. (-) denotes that fitting parameters were not applicable in the equivalent scheme used (Figs. 2 and 3).*

Material / c_{BTAH}	R_e / Ω cm^2	$Q_1 \cdot 10^6$ / Ω^{-1} s^{n}cm^{-2}	n_1	R_1 / Ω cm^2	$Q_2 \cdot 10^6$ / Ω^{-1} s^{n}cm^{-2}	n_2	R_2 / Ω cm^2	$Q_3 \cdot 10^6$ / Ω^{-1} s^{n}cm^{-2}	n_3	R_3 / Ω cm^2
Cu										
0	1.70	2.0	1.0	$1.0 \cdot 10^3$	19	0.54	$1.2 \cdot 10^4$	530	0.51	$3.2 \cdot 10^4$
0.05	7.39	1.37	0.886	$1.48 \cdot 10^4$	4.76	0.448	$4.03 \cdot 10^3$	–	–	–
10	12.2	0.366	1.0	$3.02 \cdot 10^4$	10.4	0.698	$2.65 \cdot 10^4$	826	0.63	very large
Cu-10Zn										
0	4.2	8.6	1.0	220	160	0.53	$3.2 \cdot 10^3$	660	0.53	$3.9 \cdot 10^4$
0.05	8.38	0.941	0.955	$4.74 \cdot 10^4$	2.99	0.488	$8.15 \cdot 10^5$	–	–	–
10	16.9	0.556	0.973	$9.67 \cdot 10^6$	0.372	0.67	$7.71 \cdot 10^6$	–	–	–
Cu-40Zn										
0	3.6	6.8	0.87	$4.15 \cdot 10^3$	7.5	0.42	$9.9 \cdot 10^3$	–	–	–
0.05	7.55	10.4	0.952	$1.05 \cdot 10^5$	0.107	0.632	$6.31 \cdot 10^5$	–	–	–
100	14.3	0.922	0.965	$3.27 \cdot 10^5$	0.920	0.744	$7.4 \cdot 10^5$	–	–	–
Zn										
0	9.2	25	0.86	20	110	0.90	480	–	–	–
0.05	10.6	12.5	0.73	233	10.3	0.96	$1.6 \cdot 10^3$	–	–	–
10	12.6	2.26	0.898	$7.23 \cdot 10^3$	4.14	1.0	$8.64 \cdot 10^3$	–	–	–

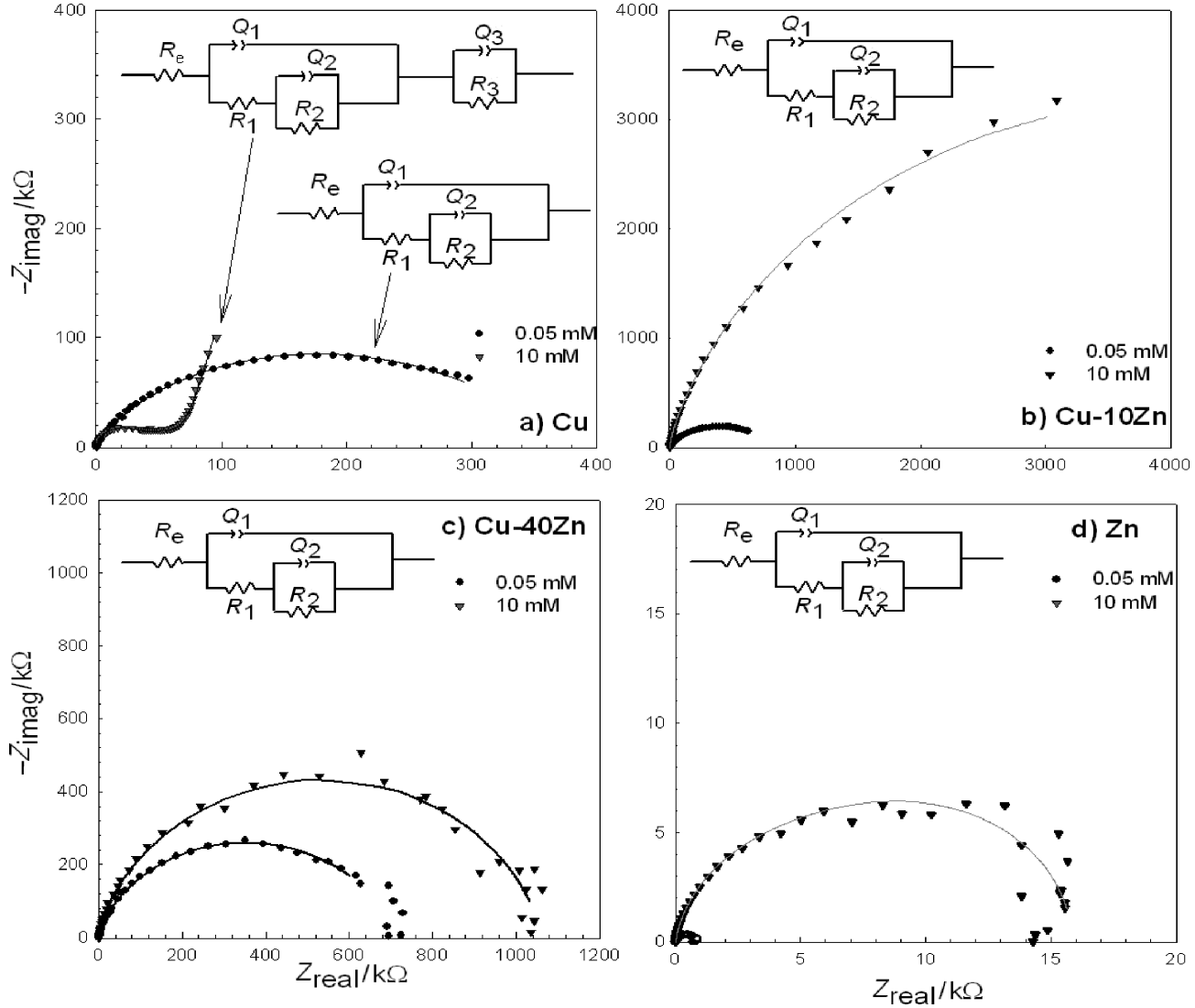

Fig. 3 – *Experimental and fitted Nyquist plots for Cu, Cu-10Zn and Cu-40Zn alloys and Zn in 0.5 M NaCl containing 0.05 mM and 10 mM BTAH after 2 h immersion. Equivalent circuits used for spectra fitting are given in the insets.*

for low concentration of inhibitor (0.05 mM BTAH) no tail is observed at low frequency range. At high concentration, however, low frequency tail appears as "blocking effect" capacitive behaviour. The fitted parameters for EIS curves given in Fig. 3 are presented in Table 2. Equivalent circuits used for fitting of experimental data in the presence of BTAH are similar to that used in chloride solution. However, the physical meaning is somewhat different. Q_1 at high frequencies reflects the capacitive properties of the film formed in the presence of BTAH.[24,25] In the middle frequency range (R_2Q_2), parameter Q_2 represents, similar to that in chloride solution, the double layer capacitance coupled with charge transfer resistance R_2 at the bottom of the pores.[24,25] In the case of Cu, the low frequency range time constant R_3Q_3 reflects a process that describes the transport through the insulating part of BTAH film. Typical capacitive behaviour of the film formed is observed and, the total polarisation resistance value is estimated to be extremely high (Table 1).

Table 2 – *Thickness, d, and inhibition efficiencies, IE, of the films formed on Cu, Cu-10Zn and Cu-40Zn alloys, and Zn after 2 h immersion in 0.5 M NaCl, and in 0.5 M NaCl containing 0.05 mM BTAH and 10 mM BTAH. d and IE were deduced from EIS data.*

Material	0.05 mM BTAH		10 mM BTAH	
	d/nm	IE/%	*d*/nm	IE/%
Cu	5.9	88.9	13.2	> 99.9
Cu-10Zn	6.0	95.0	8.2	99.7
Cu-40Zn	0.05	98.1	5.5	98.9
Zn	0.02	37.7	3.5	96.9

The capacitance of the film formed in BTAH containing solution was calculated from Q using the

equation from $C_1 = [R_1^{1-n} Q_1]^{1/n}$.[26] With increasing inhibitor concentration the parameter Q decreases (Table 1). Consequently, the capacitance C_1 is lower in the solutions containing BTAH inhibitor than in the inhibitor-free solutions for all the materials investigated. The decrease in C_1 caused by inhibitor is attributed to the formation of a polymer layer of BTAH on the electrode surface. Assuming the value for the dielectric constant of the layer, ε, the thickness of the film, d, can be evaluated from the following relationship:

$$d = (\varepsilon)\ (\varepsilon_0)\ (A)\ /\ C_1 \qquad (8)$$

where ε_0 is $8.85 \cdot 10^{-14}$ F cm^{-1} and A is surface area (cm^2). For composite organic films the chosen value of dielectric constant was 5.5, the value for dielectric constant being an average value of cuprite (7.6) or zincite (8.15) and organic film 3.[24] In previous publications other values of dielectric constants have been reported for BTAH films.[23] The estimated values of d are presented in Table 2. Thickness of the films is typically a few nm and it decreases from Cu to alloys with increasing zinc content.

Inhibition efficiency was calculated from the total polarization resistance of the system calculated as the sum of partial resistance:[27]

$$\text{IE}\ (\%) = (R_{\text{inh}} - R_{\text{uninh}})/R_{\text{inh}},$$

where R_{inh} and R_{uninh} are total resistances with and without inhibitor, respectively. The results are presented in Table 2. In the presence of 0.05 mM, the efficiency of BTAH is highest for Cu-10Zn alloy. It decreases for Cu-40Zn and Cu, athough the values are still high. In the case of Zn, IE of only 37.7 % is achieved. For 10 mM BTAH, however, high inhibition efficiency is achieved for all four materials.

X-ray photoelectron spectroscopy

XPS survey spectra recorded after 2 h immersion of Cu-10Zn alloy in 0.5 M NaCl with and without the addition of 10 mM BTAH are presented in Fig. 4. Similar results were obtained for other materials investigated. Main XPS peaks are indicated. In chloride solution, the presence of copper oxide layer was dominated by Cu LMM, Cu 2p and O1s peaks. In the presence of BTAH, the most significant change was the increase in carbon C 1s peak and the appearance of nitrogen N 1s peak. This may be explained by the incorporation of organic molecules from the inhibitor into oxide layer. More details were obtained from high resolution spectra. Normalized X-ray induced Cu and Zn Auger spectra recorded on surface layers formed on Cu, Cu-10Zn, Cu-40Zn and Zn in 0.5 M NaCl with and without addition of 10 mM BTAH are presented in Fig. 5. In 0.5 M NaCl solution, peaks re-

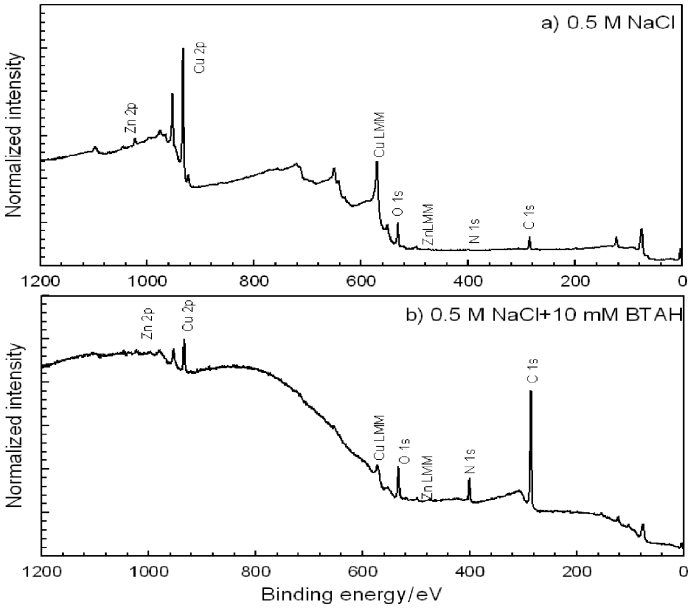

Fig. 4 – *XPS survey spectra for films formed on Cu-10Zn alloy in 0.5 M NaCl in the presence and absence of 10 mM BTAH*

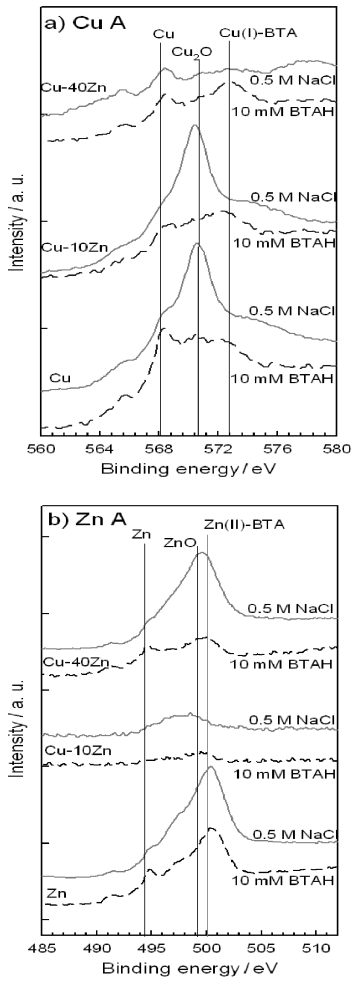

Fig. 5 – *(a) Cu and (b) Zn X-ray induced Auger spectra recorded on the surface films formed on Cu, Cu-10Zn and Cu-40Zn alloys and Zn in 0.5 M NaCl in the presence and absence of 10 mM BTAH*

lated to the metal and cuprous component were observed at 568.2 eV and 570.1 eV, respectively (Fig. 5a). The main oxidation product on Zn metal immersed in 0.5 M NaCl solution was ZnO, evidenced by the peak centred at 499.1 eV (Fig. 5b). The metal peak was located at 494.4 eV. For copper alloys the intensity of cuprous peak decreased with increasing zinc content. From the spectra given, it was evident that both metal components, copper and zinc, contributed to the formation of the oxidized surface layer formed on Cu-10Zn and Cu-40Zn alloys in chloride solution.

On BTAH-treated samples, a third component was detected in Cu Auger spectra at a binding energy of 572.6 eV (Fig. 5a), which had already been observed in the literature and ascribed to the [Cu(I)-BTA] surface polymer.[4,16,28] At the same time, the centre of the Zn oxidized component peak was shifted from 499.1 in 0.5 M NaCl solution to 500.2 eV in the presence of BTAH (Fig. 5b). Therefore, in the case of alloys, the surface layers formed evidently comprised oxide and polymer components, namely Cu_2O and ZnO oxides, and Cu(I)-BTA and Zn(II)-BTA polymers.

The in-depth composition of the layers formed in 0.5 M containing 10 mM BTAH solution was obtained by depth profiling using Ar^+ ion beam. The concentrations of individual elements as a function of sputtering time for the samples immersed in inhibitor containing chloride solution are presented in Fig. 6. The presence of Cu(I)-BTA complex is evidenced by nitrogen that persisted in the depth of the film. As mentioned above, nitrogen was present only if an organic film existed at the surface. Except for zinc metal, the curve for nitrogen and oxygen were similar indicating that both elements were present in the layer formed in the presence of BTAH. Tentative structural models are schematically presented in Fig. 6. The thickness of the inhibitor layer was estimated from the sputtering time at which the concentration of N 1s peak disappeared. The protective layer on copper consisted of a mixture of cuprous oxide and Cu(I)-BTA complex. The protective layer on Cu-10Zn alloy consisted of mixture of Cu(I)-BTA and Zn(II)-BTA complexes and both oxides Cu_2O and ZnO, as observed from Zn and Cu Auger spectra (Fig. 5). The thickness of the layer was 3.8 nm. The thickness of the polymer layer on Cu-40Zn is 4.1 nm, where ZnO slightly predominated over Cu_2O, and both complexes were found. The film on zinc was the thickest, 5.8 nm, and it consisted of ZnO and Zn(II)-BTA complex.

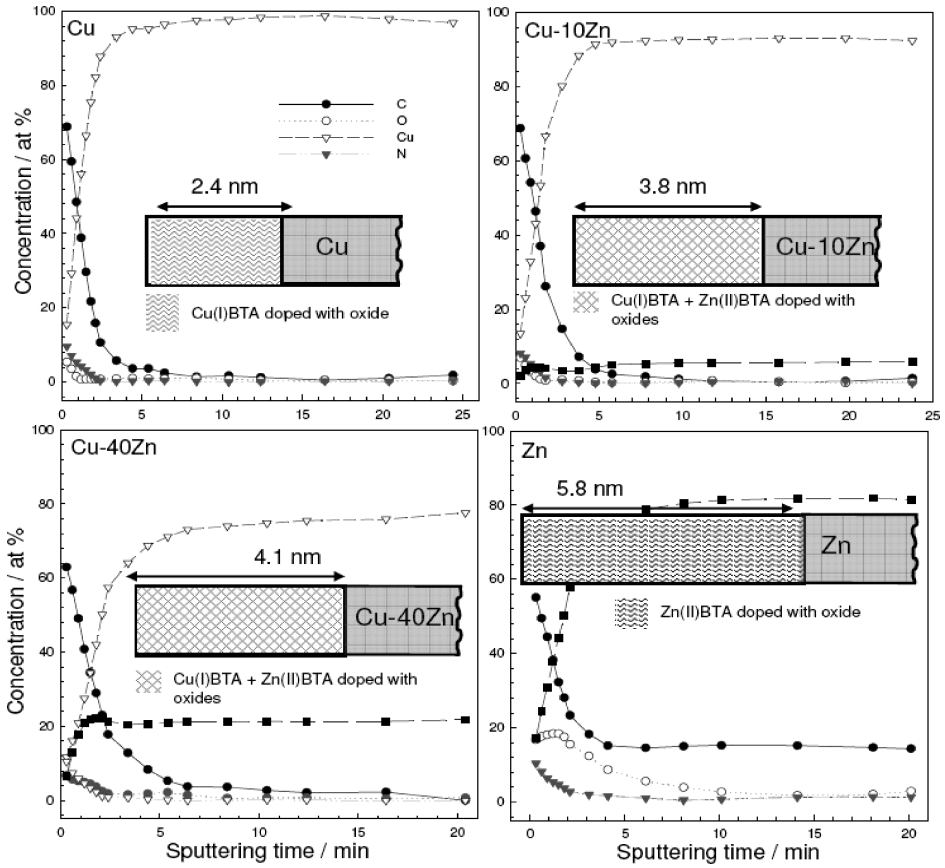

F i g . 6 – *XPS depth profiles and tentative models of the layers formed on Cu, Cu-10Zn and Cu-40Zn alloys and Zn after 2 h immersion in 0.5 M NaCl containing 10 mM BTAH. Sputtering rate 1 nm* min^{-1}.

Conclusions

Traditionally, benzotriazole is used for the inhibition of copper corrosion. This work shows that benzotriazole is a highly efficient inhibitor for copper alloys with zinc (Cu-10Zn and Cu-40Zn) as well as zinc, although for the latter to a lesser extent than for copper and the two alloys. Inhibition efficiency increases with inhibitor concentration. Based on the electrochemical impedance spectroscopy, the formation of film with high protective properties was confirmed in the presence of BTAH inhibitor. The in-depth XPS profiling enabled us to propose a tentative structure of the layers formed. The protective films on copper and zinc consisted of Cu_2O and Cu(I)-BTA polymer, and ZnO and Zn(II)-BTA polymer, respectively. The protective films formed on alloys consisted of both oxide (Cu_2O and ZnO) and both polymer (Cu(I)-BTA and Zn(II)-BTA) components.

References

1. *Mansfeld, F., Smith, T., Parry, E. P.,* Corrosion **27** (1971) 289.
2. *Walker, R.,* Corrosion **29** (1973) 291.
3. *Youda, R., Nishihara, H., Aramaki, K.,* Electrochim. Acta **35** (1990) 1011.
4. *Brusic, V., Frisch, M. A., Eldridge, B. N., Novak, F. P., Kaufman, F. B., Rush, B. M., Frankel, G. S.*, J. Electrochem. Soc. **138** (1991) 2253.
5. *Modestov, A. D., Zhou, G.-D., Wu, Y.-P., Notoya, T., Schweinsberg, D. P.,* Corros. Sci. **36** (1994) 1931.
6. *Tornkvist, C., Thierry, D., Bergman, J., Liedberg, B., Leygraf, C.,* J. Electrochem. Soc. **136** (1989) 58.
7. *Tromans, D., Sun, R.,* J. Electrochem. Soc. **138** (1991) 3235.
8. *Otmačić, H., Telegdi, J., Papp, K., Stupnišek-Lisac, E.,* J. Appl. Electrochem. **34** (2004) 5455.
9. *Finšgar, M., Lesar, A., Kokalj, A., Milošev, I.,* Electrochimica Acta **53** (2008) 8287.
10. *Mamas, S., Kiyak, T., Kabasakaloglu, M., Koc, A.,* Mater. Chem. Phys. **93** (2005) 41.
11. *Kosec, T., Milošev, I., Pihlar, B.,* Appl. Surf. Sci. **253** (2007) 8863.
12. *Hollander, O., May, R. C.,* Corrosion **41** (1985) 39.
13. *de Costa, S. L. F. A., Agostinho, S. M. L., Nobe, K.,* J. Electrochem. Soc. **140** (1993) 3483.
14. *Fenelon, M., Breslin, C. B.,* J. Appl. Electrochem. **31** (2001) 509.
15. *Sanz, J. M., Hofmann, S.,* Surf. Inter. Anal. **5** (1983) 210.
16. *Milošev, I., Strehblow, H.-H.,* J. Electrochem. Soc. **150** (2003) B517.
17. *Mannsikkamäki, K., Haapanen, U., Johans, C., Kontturi, K., Valden, M.,* J. Electrochem. Soc. **153** (2006) B311.
18. *Scendo, M.,* Corros. Sci. **47** (2005) 2778.
19. *Lee, H. P., Nobe, K.*, J. Electrochem. Soc. **133** (1986) 2035.
20. *Kabasakaloglu, M., Kiyak, T., Şendil, O., Asan, A.,* Appl. Surf. Sci. **193** (2002) 167.
21. CRC Handbook of Chemistry and Physics, *Lide, D. R.* (Ed.), 86th Edition, CRC Press, Bocaraton (2005).
22. *Raistrick, I. D., MacDonald, J. R., Francschetti, D. R.,* in *MacDonald, J. R.* (Ed.) Impedance spectroscopy Emphasizing Solid materials and Systems, John Wiley&Sons, New York, 1987, (Chapter 2).
23. *Babić, R., Metikoš-Huković, M., Lončar, M.,* Electrochim. Acta **44** (1999) 2413.
24. *Trachli, B., Keddam, M., Takenouti, H., Srhiri, A.,* Corros. Sci. **44** (2002) 997.
25. *Dermaj, A., Hajjaji, N., Joiret, S., Rahmouni, K., Srhiri, A., Takenouti, H., Vivier, V.,* Electrochim. Acta **52** (2007) 4654.
26. *Kek-Merl, D., Lappalainen J., Tuller, H. L.,* J. Electrochem. Soc. **153** (2006) J15.
27. *Scully, J. R.,* Corrosion **56** (2000) 199.
28. *Qafsaoui, W., Blanc, C., Pébčre, N., Srhiri, A., Mankowski, G.,* J. Appl. Electrochem. **30** (2000) 959.